International Journal of Engineering Trends and Technology
ISSN: 2231–5381 / https://doi.org/10.14445/22315381/IJETT-V71I6P211

Volume 71 Issue 6, 96-106, June 2023


*Original Article*

# Optimal Hybrid Image Encryption with Machine Learning Model for Blockchain-Assisted Secure Skin Lesion Diagnosis

K. Rajeshkumar[1], C. Ananth[2], N. Mohananthini[3]

[1,2]*Department of Computer and Information Science, Annamalai University, Annamalainagar, India.*
[3]*Department of Electrical and Electronics Engineering, Muthayammal Engineering College, Rasipuram, India*.

[1]*Corresponding Author : ananth.prog@gmail.com*

Received: 10 April 2023 Revised: 30 May 2023 Accepted: 07 June 2023 Published: 25 June 2023

***Abstract*** *- Skin cancer is the most prevalent ailment, which is detected initially by visual observation and further using dermoscopy analysis and other tests. The current advancement of Artificial Intelligence (AI) approaches is widely enforced for precisely identifying illnesses in real-time scenarios. Although the advantages, energy constraining, inadequately trained data, and security are the key challenges that need to be solved in the IoT-assisted healthcare field. To achieve this, blockchain (BC) technology has been newly discovered, which is the decentralized structure that has been extensively used. This study presents an Optimal Hybrid Image Encryption with Machine Learning Model for Blockchain Assisted Secure Skin Lesion Diagnosis (OHIEML-BSSLD) system. The major intention of the OHIEML-BSSLD approach is to enable a secure skin lesion detection process via image encryption and BC technology. The presented OHIEML-BSSLD technique initially enables the BC technology to store medical images securely. The OHIEML-BSSLD technique employs an advanced hybrid encryption standard with data encryption standard (HAES-DES) technique with firefly (FF) algorithm-based optimal key generation to improve the security level. For skin lesion detection, the OHIEML-BSSLD technique employs image preprocessing, fully convolutional network (FCN) based semantic segmentation, radiomics features, and optimal Kernel Extreme Learning Machine (KELM) classification. For improving the KELM model performance, the particle swarm optimization (PSO) technique was utilized for parameter tuning purposes. The performance outcome of the OHIEML-BSSLD technique was examined utilizing benchmark skin datasets, and the outputs highlighted the capable performance of the OHIEML-BSSLD technique over other techniques.*

***Keywords*** *- Medical imaging, Skin lesion diagnosis, Security, Blockchain, Image encryption, Key generation.*

## 1. Introduction

Skin disease is one of the main reasons for the global disease burden. The diagnostic criteria of skin disease generally include visual analysis of the skin lesions from their dermoscopic imageries as the first step [1]. One example was melanoma, which is life-threatening cancer. The diagnosis of melanoma involves 2 steps they are biopsy and visual inspection. To enrich the melanoma diagnosis [2], Dermoscopy can be a non-invasive skin imaging approach that attains an illuminated and extravagant image of the region of skin for amplified clarity of spots on the skin. However, the manual analysis from dermatologists' dermoscopy images can generally be time-consuming, subjective, and prone to error (even well-trained dermatologists produce commonly changing diagnostic outcomes) [3]. In this regard, automatic recognition is in highly demanded. An accurate diagnosis is crucial as some lesion types have similarities; likewise, the precision of the computer-Aided System (CAD) can be the skilled dermatologist's diagnosis [4].

Dermatologists can identify with a 65 to 85 percent accuracy rate with technology implementation. For suspect cases, dermatoscopic images were captured by a high-resolution camera to complete the visual analysis [5]. Categorizing skin lesions is the purpose of the machine learning (ML) community for a certain period. Automatic classification of lesions was utilized in medical analysis to support medical practitioners and allow affordable and rapid access to lifesaving prognosis [6], and outside of the hospital atmosphere, smartphone applications were utilized. Before 2016, many studies implemented the standard ML preprocess (enrichment) workflow, classification, feature extraction, and segmentation [7]. Computer analysis and Machine vision have become more critical to generating an effective automated melanoma diagnosis mechanism. A precise CAD system will help dermatologists and doctors be more dependable and diagnose better. Several CAD mechanisms were found by utilizing various detection, extraction, classification algorithms, and selection [8]. Some research works studies

have presented the study and analysis of image processing methods for diagnosing skin cancer; additionally, they compared Artificial Intelligence (and) and CAD system efficiency against diagnostic accuracy. Further work is remanded for minimalizing defined uncertainty in automatic Decision Support Systems (DSS) to enrich diagnosis accuracy [9].

However, in transmission and storage, there are potential threats to the important content of these images, which makes the protection of significant content a challenging issue. To gain confidentiality, encryption is a potential technology that selective encryption and full encryption [28]. Full encryption includes encrypting complete image data, while selective encryption focuses on encrypting part of image data.

This study presents an Optimal Hybrid Image Encryption with Machine Learning Model for Blockchain Assisted Secure Skin Lesion Diagnosis (OHIEML-BSSLD) technique. The presented OHIEML-BSSLD technique initially enables the BC technology to store medical images securely. The OHIEML-BSSLD technique employs an advanced hybrid encryption standard with data encryption standard (HAES-DES) technique with firefly (FF) algorithm-based optimal key generation to improve the security level.

The OHIEML-BSSLD technique employs image preprocessing, fully convolutional network (FCN) based semantic segmentation, radiomics features, and optimal Kernel Extreme Learning Machine (KELM) classification for skin lesion detection. To improve the performance of the KELM model, the particle swarm optimization (PSO) algorithm was utilized for parameter tuning purposes. The performance validation of the OHIEML-BSSLD system was examined by employing a benchmark skin dataset.

## 2. Related Works

Wang et al. [11] introduce an innovative technique called termed SSD-KD that unifies varied information as a generic KD structure for classifying skin disease. This technique modelled intra-instance relational featuring representations and integrated them with the prevailing KD study. A double relational knowledge distilled structure was self-supervised and trained in weighted softened outputs to allow the student method to capture richer knowledge from the teaching method. Khouloud et al. [12] modelled a novel DL mechanism system for detecting melanoma.

The novelty of this work was introducing 2 novels DL networking constructions, W-net, which is made up of a Feature Pyramid network and Inception-ResNet, for solving the issue of classification and the issue of segmentation—an encoder and decorder of ConvNet and ResNet. The usage of 2 concatenated encoder-decoder structures has enriched segmented outcomes.

Salma and Eltrass [13] presented an innovative, densely connected convolution network called AttDenseNet121 that can be gained by compiling the convolutional block attention module (CBAM) into DenseNet121. The optimized CBAM strengthened the representation power of DenseNet121 by suppressing unnecessary ones highlighting meaningful features, and therefore, improving the classifier performance. Kabir et al. [14] presented a novel technique for categorizing skin lesioning from not dermoscopic digitalized imageries utilizing CNN and Neutrosophic Logic SVM (CNN-NSVM) integrated method.

Ramya et al. [15] modelled a skin lesion segmented technique utilizing discrete wavelet transform for managing the complexity presented in dermoscopic imageries. The presented approach depends on examining various colour elements from several colour spaces like YCbCr and HSV exposed to discrete wavelet decomposition for removing redundant data in the procedure of colour charts, marker inks, etc.

Al-Masni et al. [16] devised a combined diagnostic structure that combined several skin cancer classification stages and skin lesion boundary segmentation steps. Initially, the authors segmented skin lesion boundaries from whole dermoscopy imageries utilizing DL full-resolution CNN (FrCN). After, a convolutional NN method was implemented to segment skin lesions for classifying purposes. A hopeful technique can be chosen by testing classification CNNs.

## 3. The Proposed Model

This research establishes an innovative OHIEML-BSSLD approach for secure skin lesion detection and classification. The major intention of the OHIEML-BSSLD system is to enable a secure skin lesion detection process via image encryption and BC technology. The presented OHIEML-BSSLD technique comprises three main procedures called BC technology, encryption, and classification. Fig. 1 demonstrates the overall flow of the OHIEML-BSSLD system.

### *3.1. BC Technology*

The presented OHIEML-BSSLD technique initially enables the BC technology to store medical images securely. Blockchain (BC) is an open and dispersed ledger taking the procedure of block lists that are designed initially for recording the transaction in a cryptocurrency system, for instance, Bitcoin [29]. It allows dependable transacting amongst a set of non-trusted participants. Lately, various types of BC platforms, like EOS, HyperLedger, and Ethereum, have been introduced and employed in different use cases. Fig. 2 defines the block diagram of BC. BC platforms can be roughly classified into three classes dependent upon the access restriction on BC users such as Consortium, Public, and Private BCs.

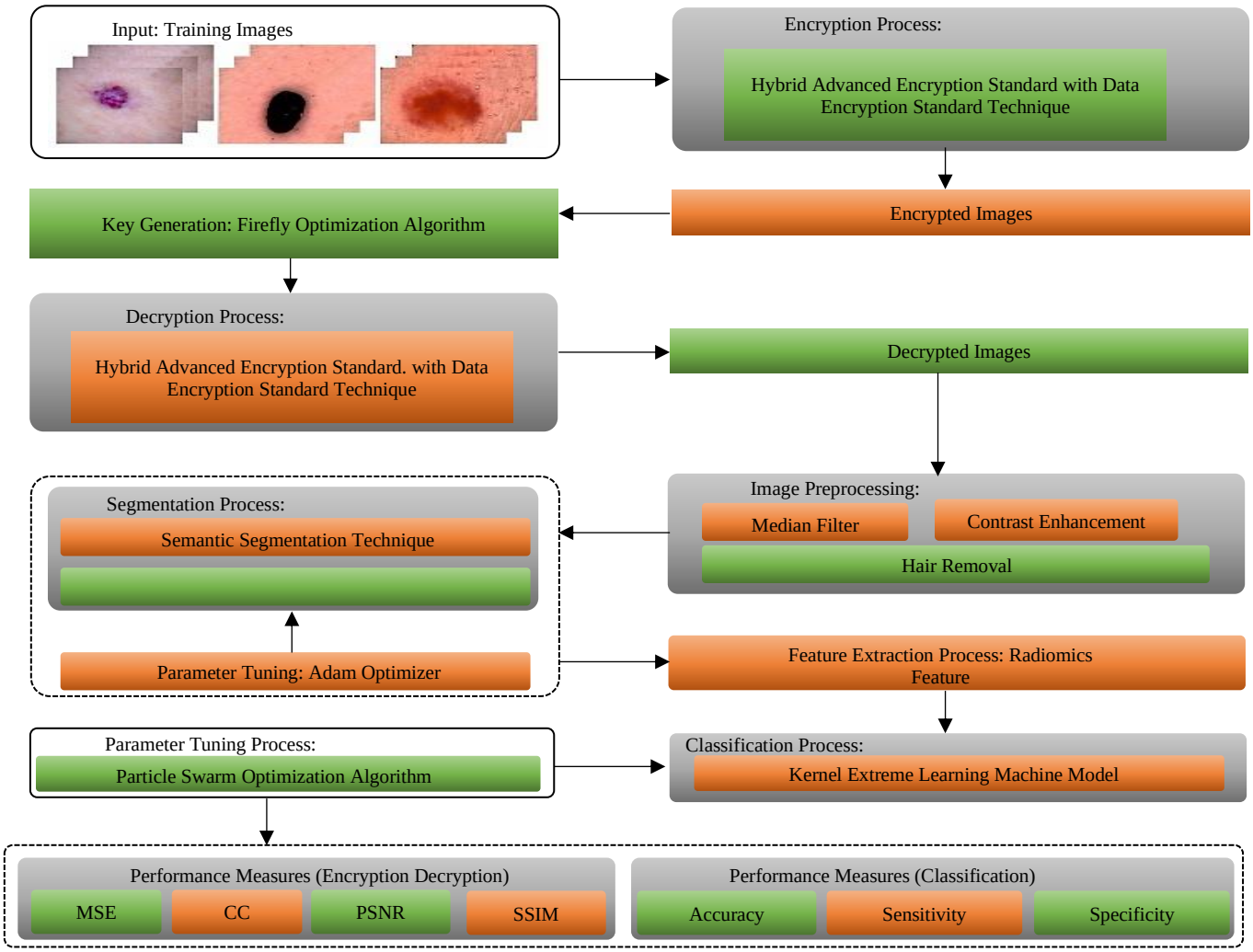


**Fig. 1 Overall flow of OHIEML-BSSLD system**

BC has different types of features, which makes them intrinsically fit for the trustworthy sharing of data:

- Decentralized. As a dispersed ledger, BC is based on P2P networking without the necessity for a central administrator or a trusted third party. Numerous models of the data record from the ledger occur in the method, which avoids data loss in case of a single point of failure.

- Tamper-Proof. BC applies consensus protocols, namely Proof-of-Work (PoW), to deal with the right to generate novel blocks. Therefore, data manipulation could not be applicable for computational overhead, making the block's data record unchangeable.

- Traceability. The transaction betwixt 2 parties in a BC could be verified simply by the rest participant. Some transactions could be tracked, and data owners might be benefitted in real-time, for example, by getting paid for all the bits of data which are utilized by 3rd party.

### *3.2. Image Encryption Procedure*

In this work, the HAES-DES algorithm is used to encrypt medical images. The fundamental concept of the presented method is to incorporate AES into all the iterations of the fiestal network of DES [18]. Every iteration of the model is mathematically modelled as follows:

$$L_n = R_{n-1} \tag{1}$$

$$R_n = AES(L_{n-1}\ xor\ R_{n-1}\ xor\ K_n) \tag{2}$$

The abovementioned expression is reiterated over the 10 rounds.

The input blocks of the 256-bit dataset are split into 2 halves, the right and the left. For every iteration $\boldsymbol{n}$, the XOR function was performed between 3 variables of the prior iteration. $(\boldsymbol{L_{n-1}}, \boldsymbol{R_{n-1}})$ and the key produced for that iteration $(\boldsymbol{K_n})$.

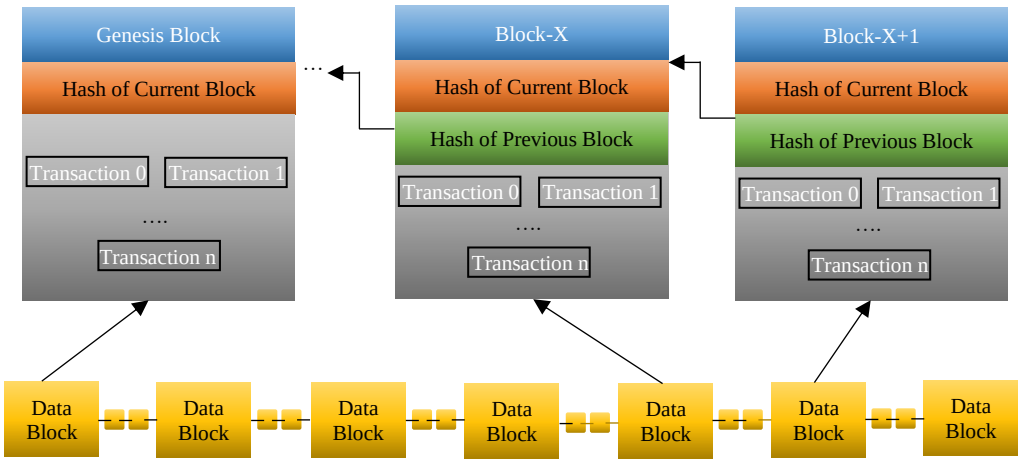


**Fig. 2 Structure of blockchain**

The outcome can be fed as input to the AES process. The outcome of the AES algorithm signifies the right half. $R_n$.The AES operation includes the shift row, mix columns byte replacement, and add round key operation. The left half of round $L_n$ is simply the earlier right half $R_{n-1}$. The above mentioned equation is repeated over 10 rounds according to the keys produced in the key scheduling task.

The key scheduling task for the presented model was adapted straightaway from the AES. To decrease the computational difficulty if different sets of keys were applied for all the standards. Also, the first and last permutation, as specified in the standard, has no security benefits. Thereby, they have been removed from the hybrid mechanism. The amount of iterations of these hybrid systems is fixed at 10. The arithmetical modeling for key extension of AES restricts the generation at 10 keys dependent upon the count of rounds employed for the 128-bit-based AES encryption technique.

The Hybrid AES-DES operation implements 10 layers of Feistel calculation using the nonlinear Eqs. (1) and (2) in addition to integrating 10 sets of AES. Accordingly, the multiple layers used for the hybrid model are set as a parameter controlled by the consumer to comply with the necessary security level.

In organizations that need improved standards of security for data and multi-media storage and transmission, the highest amount of layers of technique could be used. The inverse policy is exploited to the organization with the lowest security requirement where the different layers are decreased.

To optimally generate the keys for the HAES-DES model, the FF algorithm is used. Xin-She Yang 2007 introduced an FF algorithm which is a meta-heuristic technique simulated by the patterns of FFs and natural flashing behavior used in most Np-hard and engineering optimization problems [19]. It is a stochastic approach, viz.; a random search was utilized to find a solution. Mostly, the FF algorithm focuses on choosing the best survival solution and generating a solution within a search space. For meta-heuristic systems, exploration represents finding different solutions from the searching range, whereas exploitation represents the search phase focusing on the better adjacent solution. Algorithm 1 demonstrates the pseudocode of the FF algorithm.

The time interval and the illumination rate and mode betwixt the optical signal attract the 2 sexes to one another. The light intensity, I, reduces with enhancing distance (R) in the light source. The FF algorithm comprises three crucial features:

- The FF becomes more attractive and brighter once it moves randomly, and each representation is of a similar sex.
- The attractiveness of representing is relational to the distance and the luminance of light from it. The light absorption coefficient $\gamma$ evaluates the decrease in intensity of the light. The value of the main function defines the brightness of FF.
- The distance betwixt FFs can be attained in Eq. (3), such that $X_{i,k}$ implies the $k^{th}$part of the spatial co-ordination and $i^{th}$FFs.

$$r_{ij} = \sqrt{(xi - xj)^2 + (yi - yj)^2} \tag{3}$$

The movement of FFs and attractiveness towards a brighter FF is defined as follows:

$$X_i = X_i + B_0 e^{rij^2}\left(X_j - X_i\right) + a\left(rand - \frac{1}{2}\right) \tag{4}$$

Where $a$ denotes a randomizer parameter, $rand$ indicates a value within [0,1] generated randomly, and $B$ shows the attractiveness of the light source. The attractiveness changes define the variable $\gamma$.

**Algorithm 1:** Pseudocode of the FA

Start
Produce the first populace of FFs $X_i(i = 1 \ldots N)$
Initializing parameters: $\alpha, \gamma, \beta_{\min}$, and $t = 0$, and Fes $= 0$
Brightness $1_i$ at $X_i$ can be defined by $(X_i)$ ;
Determine the captivation of light co-efficient $\gamma$;
While (not meeting the stopping criteria)
For $i = 1$: N each N FF
  For j $= 1$: $N$, each $N$ FFs
    $If\ I_j > I_i$ Then
      Move FF $i$ nearby j in every dimensional dependent upon Eq. (4);
    EndIf
      Attractiveness changes with distance;
      Calculate the newly generated solution and upgrade the brightness; Fes $= Fes + 1$;
    EndFor
  EndFor
Find the current best and rank the FFs;
$t = t + 1$;
EndWhile
Post-process result.
End

Now, the optimum key sets are chosen by considering fitness as the maximal key using PSNR for unscrambled and scrambled data from medicinal images. The objective function was presented by using the FF algorithm as follows.

$$Fitness = MAX\{PSNR\} \quad (5)$$

### *3.3. Skin Lesion Classification Procedure*

For skin lesion detection, the OHIEML-BSSLD technique encompasses preprocessing, FCN-based semantic segmentation, radiomics features, KELM classification, and PSO-based parameter tuning.

#### *3.3.1. Image Preprocessing*

The introduced OHIEML-BSSLD approach performs a noise removal process using a median filter. Then, the noise removal images undergo a contrast enhancement process using the CLAHE technique. Finally, an inpainting technique is employed for the noise-removal process. Inpainting can be used to remove hairs from the skin in an image or video. The process involves identifying the hairs in the image and analyzing the surrounding area to synthesize a new version of the image with the hairs removed.

#### *3.3.2. Semantic Segmentation*

For image segmentation, the FCN model is used. An FCN was trained for mapping from the RGB input to the posterior probability map [20]. The network encompasses 19 layers with 290 and 129 trained parameters. The stride is fixed as 1 and utilizes ReLU as an activation function for all the convolution or deconvolution layers. Pixel-wise classifier can be implemented, and FCN was acted as filtering, which tasks the whole input images to the map. However, every component signifies the possibility that the respective input pixel goes to the tumour. With the consecutive pooling and convolutional layers, CNN could incorporate context data from the regional to global scales, which leads to decreased resolution in the output layer.

On the other hand, image segmentation is used to classify all the pixels into foreground or background alongside full-resolution output. To resolve these conflicts between full-resolution pixel-wise classification and multiscale information aggregation, the study implemented an approach of using deconvolutional and upsampling layers for recovering the lost resolution when transferring the global perception from the pooling layer. The upsampling layer executes the reversing function of pooling and reconstructing the unique magnitude of activations. The deconvolution layers constrict the activation of the coarse maps attained in upsampling through a swap of the forward as well as backward passes of the convolutional, thereby a single input activation has been proposed into more than one output after deconvolution, which yields expanded and dense feature maps.

A hierarchical system of deconvolution layers was utilized for recovering image details at various levels, where the low layer encodes the image data and the high layer captures fine details with respect to skin cancers. Thus, the network considered fine details and global information for the segmentation of tumors.

The tuning process of the FCN approach was achieved by Adaptive Moment Estimation (ADAM) optimization. ADAM is an optimizing approach implemented in ML and DL techniques to update the model's parameters. It is an alternative to stochastic gradient descent (SGD) that exploits an adaptive learning rate that implies the learning rate can be adjusted for all the parameters based on the historical gradient value. Adam works by preserving an exponentially weighted average of the past gradient and past squared gradients. They are used to calculate an adaptive learning rate for all the parameters that assist in avoiding oscillations or divergences and help the model converge more quickly.

#### *3.3.3. Radiomics Features*

The radiomics feature is derived from in-house software, with the help of PyRadiomics and Python's skit-learning package [21]. The 3 types of characteristics that are evaluated namely intensity, Shape, and Texture. 26 shape and 19 intensity-based features are extracted for all the extraction settings, such as bin, width, bin, and contour, with 16 discrete settings that could be permutations of two filters (LoG and original), 2 contours (Gold and HGG), bandwidth (2, 4, 8, 16), and 1450 overall quantity of derived radiomics imaging features.

*3.3.4. Optimal KELM-based Classification*

Finally, for the skin lesions classification, the KELM approach was utilized. Huang et al. developed a new ELM named KELM by presenting kernel function as the original ELM [22]. Especially, KELM has stable and excellent performance as well as inherits the benefits of the ELM like great fast learning speed and generalization performance. The ELM can be mathematically modelled as:

$$f(x) = h(x)H^T(\frac{I}{c} + HH^T)^{-1}T \quad (6)$$

In Eq. (6), $\chi$ indicates the input sample, $h(x)$ and $H$ denotes the hidden state feature map matrices.

In this work, kernel function $K(u,v)$ proceeds the location of $H$, together with $h(x)$ and $H$, the relationships betwixt input as well as output are given the matrix form

$$f(x) = h(x)H^T(\frac{I}{c} + HH^T)^{-1}T$$
$$= \begin{bmatrix} K(x,x_1) \\ \vdots \\ K(x,x_N) \end{bmatrix}(\frac{I}{c} + \Omega_{KELM})^{-1}T \quad (7)$$

Let $\Omega_{KELM}$ be the kernel matrix that is given in Eq. (8):

$$\begin{cases} \Omega_{KELM} = HH^T \\ \Omega_{KELMi,j} = h(x_j) \times h(x_j) = K(x_i,x_j) \end{cases} \quad (8)$$

Additionally, the kernel function contains linear, polynomial, and Radial Basis Function, where the Gaussian Kernel Function has widely utilized kernel model from KELM, as follow:

$$K(,v) = \exp(-\gamma||u - v|||^2) \quad (9)$$

From the Eqs. (7)- (9), $C$ and $\gamma$ denote the KELM's key parameters, significantly impacting the model's efficacy.

To adjust the KELM parameters, the PSO algorithm is exploited. PSO algorithm is based on the swarming of $N$ individuals called particles, each representing a solution to problems with $D$ dimension [23]. Its genotype encompasses $2D$ parameters, with the initial $D$ parameters representing the coordinate of particle position and the last $D$ parameter as its velocity component in the $D$-dimension problem space. Besides the two essential properties, the subsequent properties are: $gbest$ global better position of the entire swarm and $pbest_i$ personal optimal location of each particle in the search spaces. The FF corresponding to the problem exploited for assessing the (goodness" of each particle):

$$v_i^{(t+1)} = \omega v_i^{(t)} + c_1 r_1 \left(pbest_i^{(t)} - p_i^{(t)}\right) + c_2 r_2 \left(gbest^{(t)} - p_i^{(t)}\right) \quad (10)$$

$$p_i^{(t+1)} = p_i^{(t)} + v_i^{(t+1)} \quad (11)$$

Where, $p_i^{(t)}$ and $v_i^{(t)}$ correspondingly specifies the location and velocity of $i^{th}$ particles at $t^{th}$ iterations. $c_1$ and $c_2$ are the two positive factors of cognitive and social coefficients, which controls the contribution of $pbest_i$ (cognitive component) local better solution and $gbest$ (social component) the better global solution, correspondingly. $r_1$ and $r_2$ demonstrates the two independent random parameters within [0,1]. The inertia-weighted factor $\omega$ is exploited to control the swarm convergence. In this work, a non-linear altering inertia factor for SSPSO and PSO is employed:

$$\omega = \omega_{\max} - \frac{(\omega_{\max} - \omega_{\min})t}{T_{\max}} \quad (12)$$

In Eq. (12), $T_{\max}$ represents the maximal iteration count, and $t$ represents the existing number of iterations. At the iteration, every dimension of velocity is defined within $[-V_{\max}, V_{\max}]$ to limit the maximal distance that particle will move.

The PSO presents an FF to realize great classifier efficiency. It describes a positive integer for signifying a better candidate result performance. The minimization of an error rate of the classifier assumed as FF is expressed below:

$$fitness(x_i) = ClassifierErrorRate(x_i)$$
$$= \frac{no.of\ misclassified\ instances}{Total\ no.of\ instances} * 100 \quad (13)$$

## 4. Results and Discussion

The suggested technique is put under simulation by employing Python 3.6.5 tool on PC i5-8600k, 250GB SSD, GeForce 1050Ti 4GB, 16GB RAM, and 1TB HDD. The setups of the parameter are provided in the following: learning rate: 0.01, activation: ReLU, epoch count: 50, dropout: 0.5, and size of the batch: 5.

**Table 1. Encryption outcomes of OHIEML-BSSLD approach with distinct classes**

| Number of Classes | MSE | PSNR (dB) | Correlation Coefficient | SSIM |
|---|---|---|---|---|
| Angioma | 0.5418 | 52.7117 | 0.9816 | 0.8827 |
| Basal Cell Carcinoma | 0.7031 | 51.4236 | 0.9686 | 0.8519 |
| Lentigo NOS | 0.7093 | 51.4580 | 0.9482 | 0.8300 |
| Melanoma | 0.6937 | 51.5369 | 0.9764 | 0.8341 |
| Nevus | 0.7292 | 51.3186 | 0.9636 | 0.8255 |
| Seborrheic Keratosis | 0.7036 | 51.3635 | 0.9717 | 0.8555 |
| Solar Lentigo | 0.7000 | 51.4912 | 0.9490 | 0.8417 |
| **Overall** | **0.6829** | **51.6148** | **0.9656** | **0.8459** |

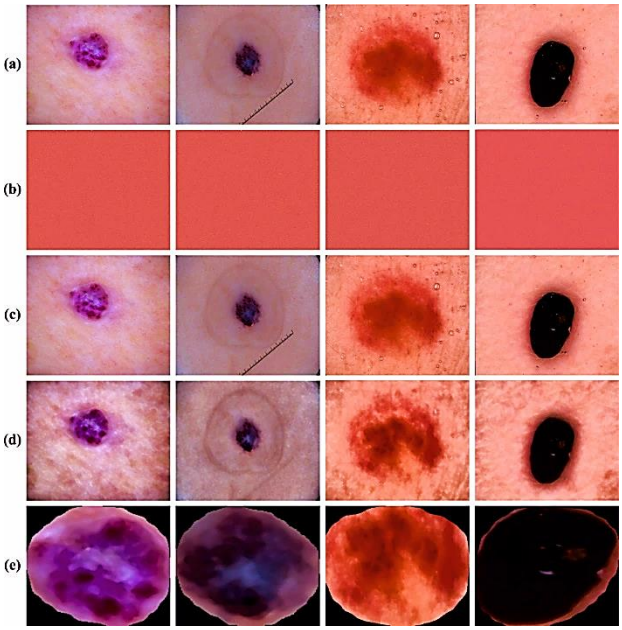


**Fig. 3 Images a) Original b) Encrypted c) Decrypted d) Preprocessed e) Segmented**

In this segment, the experimental outcome of the OHIEML-BSSLD technique was investigated on the ISIC skin lesion database [24]. Fig. 3 illustrates some sample images.

In Table 1 and Fig. 4, the encryption outputs of the OHIEML-BSSLD algorithm are well investigated under different classes. The results referred that the OHIEML-BSSLD technique attains an effectual outcome on the encryption process. For instance, in the angioma class, the OHIEML-BSSLD technique achieves 0.5418: MSE, 52.7117dB: PSNR, 0.9816: CC, and 0.8827: SSIM. Simultaneously, on the melanoma class, the OHIEML-BSSLD algorithm gains 0.6937: MSE, 51.5369dB: PSNR, 0.9764: CC, and 0.8341: SSIM.

Concurrently, on the nevus class, the OHIEML-BSSLD algorithm gained 0.7292: MSE, 51.3186dB: PSNR, 0.9636: CC, and 0.8255: SSIM. Finally, in the solar lentigo class, the OHIEML-BSSLD method attained 0.7000: MSE, 51.4912dB: PSNR, 0.9490: CC, and 0.8417: SSIM.

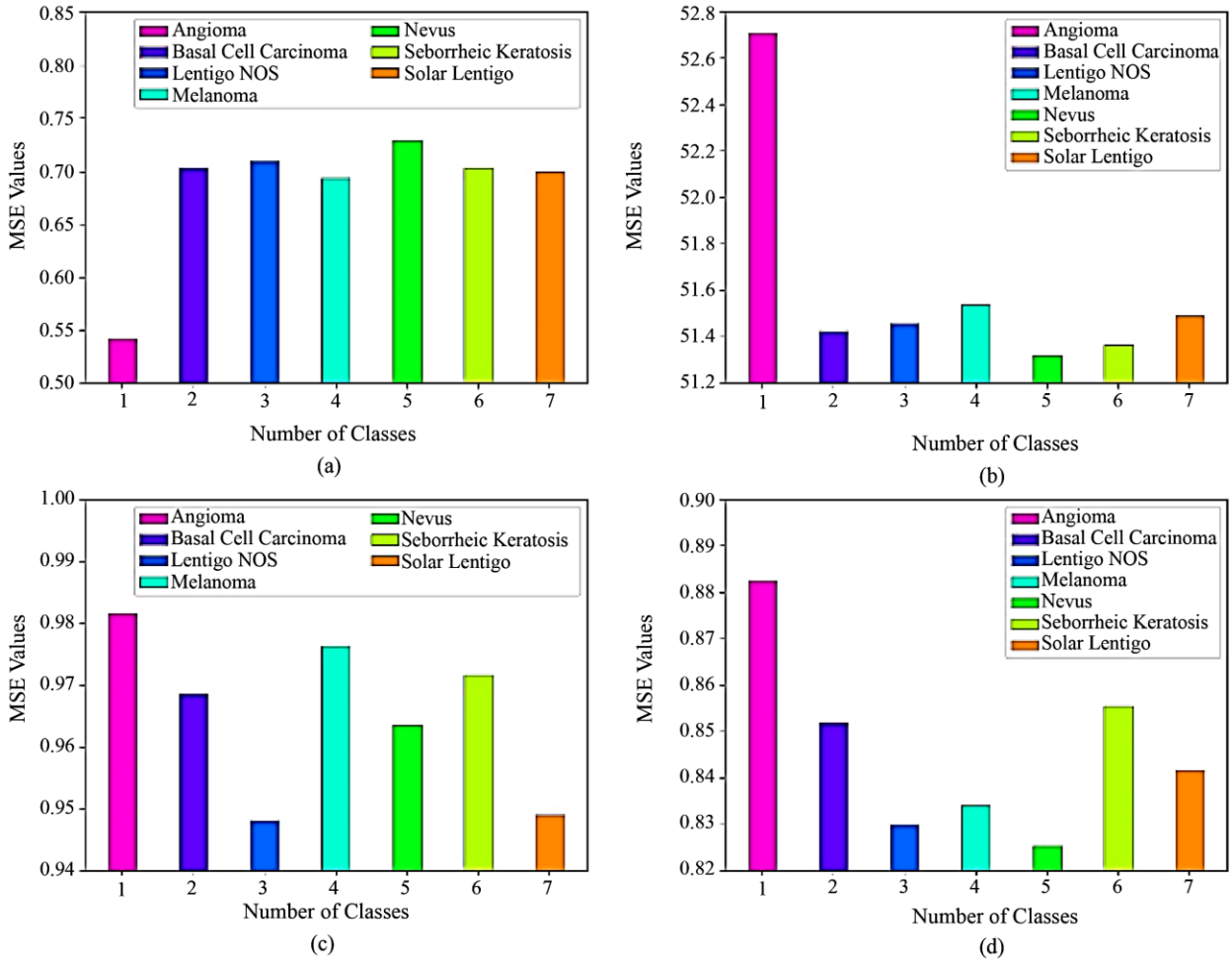


**Fig. 4 Encryption outcomes of OHIEML-BSSLD approach (a) MSE, (b) PSNR, (c) CC, and (d) SSIM**

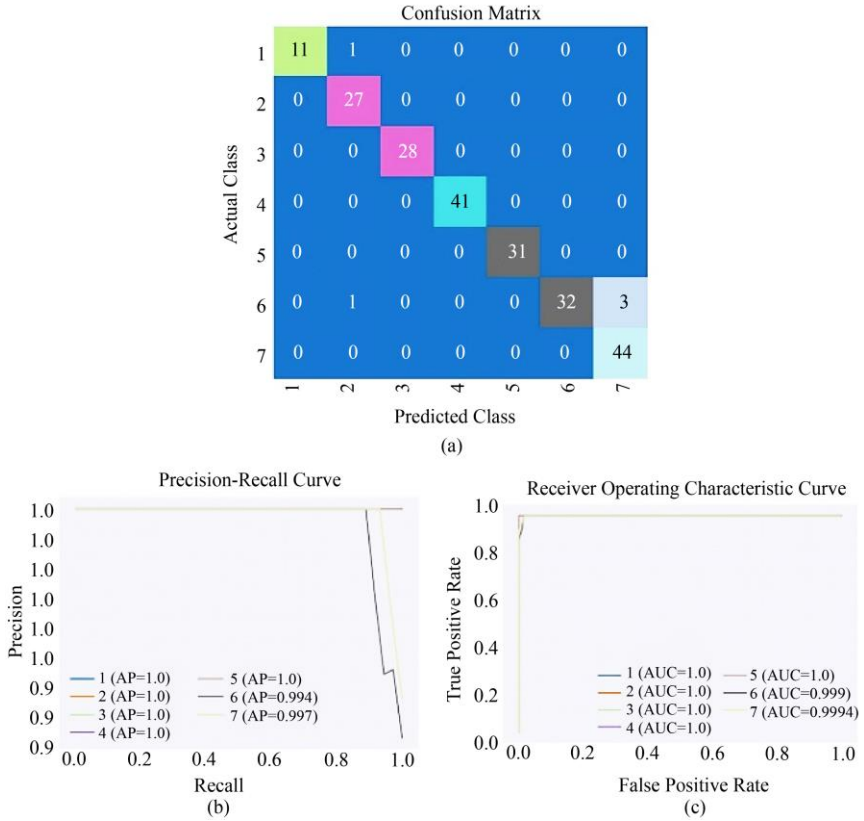


**Fig. 5 Classifier outcome of the training dataset (a) Confusion matrix, (b) PR, and (c) ROC**

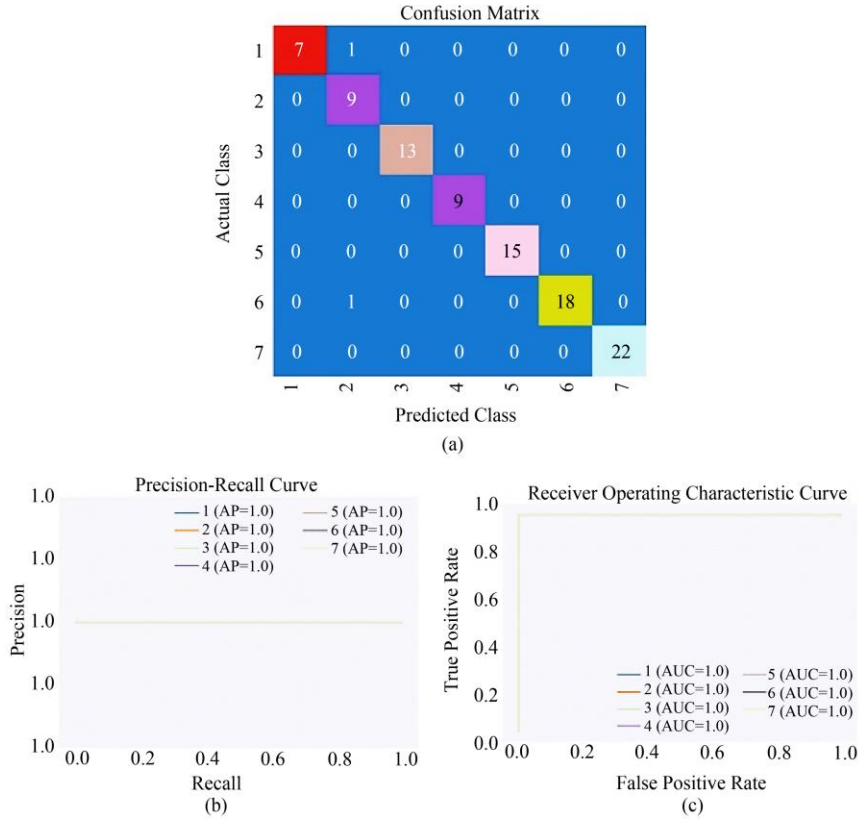


**Fig. 6 Classifier outcome of the testing dataset (a) Confusion matrix, (b) PR, and (c) ROC**

**Table 2. TRS and TSS analysis of the OHIEML-BSSLD approach**

| Measures | Training Set | Testing Set |
|---|---|---|
| Accuracy | 97.72 | 98.94 |
| Sensitivity | 97.22 | 98.57 |
| Specificity | 99.61 | 99.81 |

Fig. 5 exhibits the classifier outcomes of the OHIEML-BSSLD approach under the training dataset. Fig. 5a represents the confusion matrices presented by the OHIEML-BSSLD method. The figure stated that the OHIEML-BSSLD method had recognized 11, 27, 28, 41, 31, 32, and 44 instances under classes 1-7. Also, Fig. 5b determines the PR examination of the OHIEML-BSSLD approach. The figures described that the OHIEML-BSSLD approach had obtained greater PR achievement under seven classes. Lastly, Fig. 5c describes the ROC study of the OHIEML-BSSLD algorithm. The figure depicted that the OHIEML-BSSLD algorithm has given an outcome in capable outcomes with enhanced ROC values under seven classes.

Fig. 6 establishes the classifier outcome of the OHIEML-BSSLD approach under the training dataset. Fig. 6a represents the confusion matrices presented by the OHIEML-BSSLD model. The figure presented that the OHIEML-BSSLD model has recognized 7, 9, 13, 9, 15, 18, and 22 instances under classes 1-7. Likewise, Fig. 6b demonstrates the PR analysis of the OHIEML-BSSLD model. The figures reported that the OHIEML-BSSLD algorithm had obtained maximal PR performance under seven classes. Lastly, Fig. 6c depicts the ROC examination of the OHIEML-BSSLD methodology.

In Table 2 and Fig. 7, the comprehensive outcome of the OHIEML-BSSLD technique is investigated on TRS and TSS. The results indicate that the OHIEML-BSSLD technique reaches effectual outcomes under TRS and TSS.

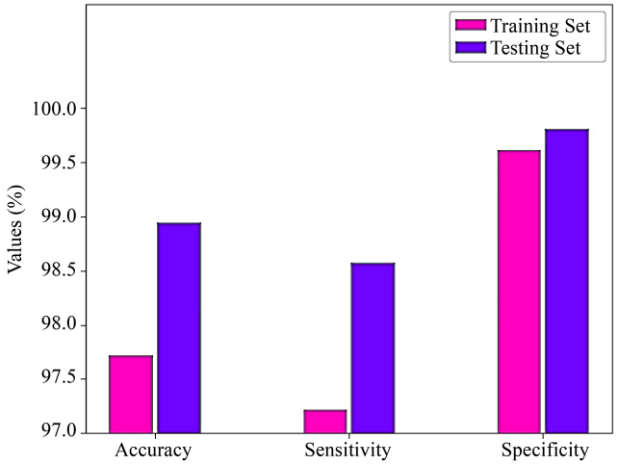


**Fig. 7 TRS and TSS analysis of OHIEML-BSSLD technique**

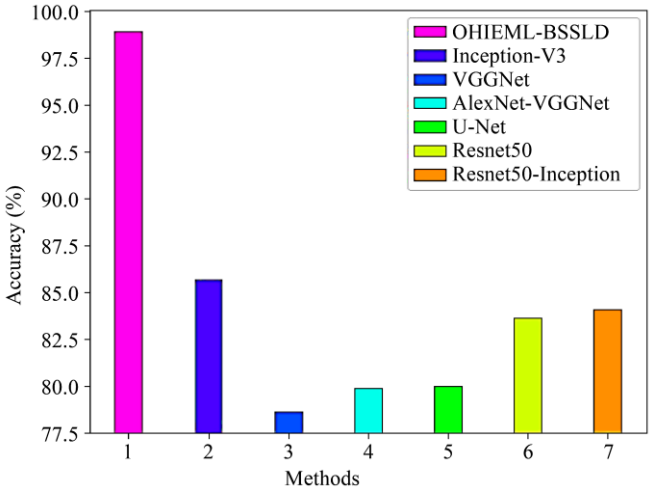


**Fig. 8 $Accu_y$ evaluation of OHIEML-BSSLD technique with other algorithms**

For instance, on TRS, the OHIEML-BSSLD technique obtains $accu_y$ of 97.72%, $sens_y$ of 97.22%, and $spec_y$ of 99.61%. Besides, on TSS, the OHIEML-BSSLD system gains $accu_y$ of 98.94%, $sens_y$ of 98.57%, and $spec_y$ of 99.81%.

In Table 3, an elaborative relational investigation of the OHIEML-BSSLD technique takes place [25, 26]. Fig. 8 demonstrates the performance of the OHIEML-BSSLD algorithm with other methods by means of $accu_y$. The outputs indicate that the OHIEML-BSSLD technique gains increasing performance. Based on $accu_y$, the OHIEML-BSSLD technique achieves higher $accu_y$ of 98.94% while the Inception-v3, VGGNet, AlexNet-VGGNet, U-Net, Resnet50, and Resnet50-Inception models accomplish reduced $accu_y$ of 85.70%, 78.60%, 79.90%, 80%, 83.60%, and 84.10% respectively.

**Table 3. Relative result of OHIEML-BSSLD technique with other methods [25, 26]**

| Methods | $Accu_y$ | $Sens_y$ | $Spec_y$ |
|---|---|---|---|
| OHIEML-BSSLD | 98.94 | 98.57 | 99.81 |
| Inception-V3 | 85.70 | 86.46 | 86.06 |
| VGGNet | 78.60 | 79.60 | 79.68 |
| AlexNet-VGGNet | 79.90 | 80.35 | 80.47 |
| U-Net | 80.00 | 79.43 | 78.92 |
| Resnet50 | 83.60 | 84.89 | 85.14 |
| Resnet50-Inception | 84.10 | 84.25 | 84.09 |

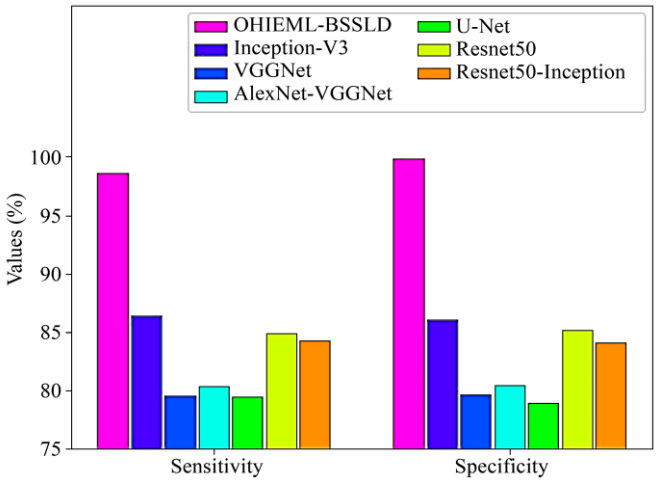


**Fig. 9 $Sens_y$ and $spec_y$ evaluation of OHIEML-BSSLD technique with other algorithms**

Fig. 9 depicts the performance of the OHIEML-BSSLD algorithm with other approaches in terms of $sens_y$ and $spec_y$. The outcomes inferred that the OHIEML-BSSLD algorithm attains greater performance. With respect to $sens_y$, the OHIEML-BSSLD approach accomplishes maximal $sens_y$ of 98.57% while the Inception-v3, VGGNet, AlexNet-VGGNet, U-Net, Resnet50, and Resnet50-Inception methodologies achieve lesser $sens_y$ of 86.46%, 79.60%, 80.35%, 79.43%, 84.89%, and 84.25% correspondingly.

Followed by, in terms of $spec_y$, the OHIEML-BSSLD system obtains enhanced $spec_y$ of 99.81% while the Inception-v3, VGGNet, AlexNet-VGGNet, U-Net, Resnet50, and Resnet50-Inception methodologies achieve minimal $spec_y$ of 86.06%, 79.68%, 80.47%, 78.92%, 85.14%, and 84.09% correspondingly. These outcomes highlighted the improved performance of the OHIEML-BSSLD technique.

## 5. Conclusion

This study establishes a novel OHIEML-BSSLD technique for secure skin lesion detection and classification. The major intention of the OHIEML-BSSLD approach is to enable a secure skin lesion detection process via image encryption and BC technology. The presented OHIEML-BSSLD technique initially enables the BC technology to store medical images securely. The OHIEML-BSSLD technique employed the HAES-DES technique with FF algorithm-based optimal key generation to improve the security level. For skin lesion detection, the OHIEML-BSSLD technique encompasses preprocessing, FCN-based semantic segmentation, radiomics features, KELM classification, and PSO-based parameter tuning. The performance result of the OHIEML-BSSLD system was tested using benchmark skin databases, and the outcomes pointed out the promising performance of the OHIEML-BSSLD algorithm over other algorithms. In future, ensemble DL classifiers will be employed to increase the detection rate.

## References

[1] Selvia et al., "Skin Lesion Detection Using Feature Extraction Approach," *Annals of the Romanian Society for Cell Biology*, vol. 25, no. 4, pp. 3939-3951, 2021.[Google Scholar] [Publisher Link]

[2] Jwan Najeeb Saeed, and Subhi R. M. Zeebaree, "Skin Lesion Classification Based on Deep Convolutional Neural Networks Architectures," *Journal of Applied Science and Technology Trends*, vol. 2, no. 1, pp. 41-51, 2021. [CrossRef] [Google Scholar] [Publisher Link]

[3] S. Naresh Kumar, and B. Mohammed Ismail, "Systematic Investigation on Multi-Class Skin Cancer Categorization Using Machine Learning Approach," *Materials Today: Proceedings*, 2020. [CrossRef] [Google Scholar] [Publisher Link]

[4] MD Khairul Islam, Chetna Kaushal, and MD Al Amin, "Smart Home-Healthcare for Skin Lesions Classification with IoT Based Data Collection Device," *TechRxiv, IEEE Access*, vol. 4, pp. 1-11, 2021. [CrossRef] [Google Scholar] [Publisher Link]

[5] Seena Joseph, and Oludayo O. Olugbara, "Preprocessing Effects on Performance of Skin Lesion Saliency Segmentation," *Diagnostics*, vol. 12, no. 2, pp. 344, 2022. [CrossRef] [Google Scholar] [Publisher Link]

[6] D. Naveen Raju, Hariharan Shanmugasundaram, and D. Yuvaraj, "Hybrid Approach for Melonama Detection in Dermoscopic Images," *Materials Today: Proceedings*, 2021. [CrossRef] [Google Scholar] [Publisher Link]

[7] Nithya Anoo et al., "An Efficient Skin Cancer Classification Approach Using Neural Networks," *Journal of Algebraic Statistics*, vol. 13, no. 3, pp. 4946-4957, 2022.[Google Scholar] [Publisher Link]

[8] Shubham Gupta, "An Anatomization for Classification Skin Lesion Using Custom CNN Framework," *International Conference on Industrial Electronics Research and Applications (ICIERA)*, pp. 1-6, 2021. [CrossRef] [Google Scholar] [Publisher Link]

[9] Jing Wu et al., "A Multi-Input CNNs with Attention for Skin Lesion Classification," *IEEE International Conference on Smart Cloud*, pp. 78-83, 2020. [CrossRef] [Google Scholar] [Publisher Link]

[10] T. Tamilselvi et al., "Deep Derma Scan: A Proactive Diagnosis System for Predicting Malignant Skin Tumor with Deep Learning Mechanisms," *International Journal of Engineering Trends and Technology*, vol. 70, no. 8, pp. 310-317, 2022. [CrossRef] [Publisher Link]

[11] Yongwei Wang et al., "SSD-KD: A Self-Supervised Diverse Knowledge Distillation Method for Lightweight Skin Lesion Classification Using Dermoscopic Images," *Medical Image Analysis*, vol. 84, 2023. [CrossRef] [Google Scholar] [Publisher Link]

[12] Sahib Khouloud et al., "W-Net and Inception Residual Network for Skin Lesion Segmentation and Classification," *Applied Intelligence*, vol. 52, no. 4, pp. 3976-3994, 2022. [CrossRef] [Google Scholar] [Publisher Link]

[13] Wessam Salma, and Ahmed S. Eltrass, "Automated Deep Learning Approach for Classification of Malignant Melanoma and Benign Skin Lesions," *Multimedia Tools and Applications*, vol. 81, pp. 32643–32660, 2022. [CrossRef] [Google Scholar] [Publisher Link]

[14] Md. Mohsin Kabir et al., "CNN-NSVM Architecture for Skin Lesion Classification Using Non-Dermoscopic Digital Image," *Joint 10th International Conference on Informatics, Electronics & Vision (ICIEV) and 2021 5th International Conference on Imaging, Vision & Pattern Recognition (icIVPR)*, pp. 1-7, 2021. [CrossRef] [Google Scholar] [Publisher Link]

[15] J. Ramya, H.C. Vijaylakshmi, and Huda Mirza Saifuddin, "Segmentation of Skin Lesion Images Using Discrete Wavelet Transform," *Biomedical Signal Processing and Control*, vol. 69, 2021. [CrossRef] [Google Scholar] [Publisher Link]

[16] Mohammed A. Al-masni, Dong-Hyun Kim, and Tae-Seong Kim, "Multiple Skin Lesions Diagnostics via Integrated Deep Convolutional Networks for Segmentation and Classification," *Computer Methods and Programs in Biomedicine*, vol. 190, 2020. [CrossRef] [Google Scholar] [Publisher Link]

[17] Vedant Bhatt, and Mohammad Makki, "Artificial Intelligence for Curing Skin Disorders," *SSRG International Journal of Computer Science and Engineering*, vol. 5, no. 10, pp. 7-9, 2018. [CrossRef] [Publisher Link]

[18] Anurhea Dutta et al., "Hybrid AES-DES Block Cipher: Implementation using Xilinx ISE 9.1 i.," *International Conference on Advances in Electronics and Electrical*, pp. 1-5, 2012. [CrossRef] [Google Scholar] [Publisher Link]

[19] Mina Javanmard Goldanloo, and Farhad Soleimanian Gharehchopogh, "A hybrid OBL-based Firefly Algorithm with Symbiotic Organisms Search Algorithm for Solving Continuous Optimization Problems," *The Journal of Supercomputing*, vol. 78, no. 3, pp. 3998-4031, 2022. [CrossRef] [Google Scholar] [Publisher Link]

[20] Yading Yuan, Ming Chao, and Yeh-Chi Lo, "Automatic Skin Lesion Segmentation Using Deep Fully Convolutional Networks with Jaccard Distance," *IEEE Transactions on Medical Imaging*, vol. 36, no. 9, pp. 1876-1886, 2017. [CrossRef] [Google Scholar] [Publisher Link]

[21] Jing Qian et al., "Prediction of MGMT Status for Glioblastoma Patients Using Radiomics Feature Extraction from 18F-DOPA-PET Imaging," *International Journal of Radiation Oncology* Biology* Physics*, vol. 108, no. 5, pp. 1339-1346, 2020. [CrossRef] [Google Scholar] [Publisher Link]

[22] Jie Luo et al., "A New Kernel Extreme Learning Machine Framework for Somatization Disorder Diagnosis," *IEEE Access*, vol. 7, pp. 45512-45525, 2019. [CrossRef] [Google Scholar] [Publisher Link]

[23] Yun Hou et al., "A Multi-Objective Discrete Particle Swarm Optimization Method for Particle Routing in Distributed Particle Filters," *Knowledge-Based Systems*, vol. 240, 2022. [CrossRef] [Google Scholar] [Publisher Link]

[24] ISIC Challenge Datasets. [Online]. Available: https://challenge.isic-archive.com/data/

[25] U. Padmavathi, and Narendran Rajagopalan, "Blockchain Enabled Emperor Penguin Optimizer Based Encryption Technique for Secure Image Management System," *Wireless Personal Communications*, vol. 127, pp. 2347-2364, 2022. [CrossRef] [Google Scholar] [Publisher Link]

[26] Walaa Gouda et al., "Detection of Skin Cancer Based on Skin Lesion Images Using Deep Learning," *Healthcare*, vol. 10, no. 7, 2022. [CrossRef] [Google Scholar] [Publisher Link]

[27] Soumya Gadag, and P. Pradeepa, "A Critical Literature Review on Computer Vision Based Melanoma Detection and Identification," *SSRG International Journal of Electrical and Electronics Engineering*, vol. 9, no. 12, pp. 59-80, 2022. [CrossRef] [Publisher Link]

[28] Vipul M Dabhi et al., "Detection and Classification of Skin Cancer using Back Propagated Artificial Neural Networks," *JES-Journal of Engineering Sciences*, vol. 12, no. 6, pp. 686-693, 2021. [Google Scholar] [Publisher Link]

[29] Jei Young Lee, "A Decentralized Token Economy: How Blockchain and Cryptocurrency Can Revolutionize Business," *Business Horizons*, vol. 62, no. 6, pp. 773-784, 2019. [CrossRef] [Google Scholar] [Publisher Link]